Exp Brain Res (2015) 233:459–476
DOI 10.1007/s00221-014-4127-2

RESEARCH ARTICLE

A mechanism for decision rule discrimination by supplementary eye field neurons

Supriya Ray · Stephen J. Heinen

Received: 13 August 2014 / Accepted: 11 October 2014 / Published online: 5 November 2014

Abstract A decision to select an action from alternatives is often guided by rules that flexibly map sensory inputs to motor outputs when certain conditions are satisfied. However, the neural mechanisms underlying rule-based decision making remain poorly understood. Two complementary types of neurons in the supplementary eye field (SEF) of macaques have been identified that modulate activity differentially to interpret rules in an ocular go–nogo task, which stipulates that the animal either visually pursue a moving object if it intersects a visible zone ('go'), or maintain fixation if it does not ('nogo'). These neurons discriminate between go and nogo rule-states by increasing activity to signal their preferred (agonist) rule-state and decreasing activity to signal their non-preferred (antagonist) rule-state. In the current study, we found that SEF neurons decrease activity in anticipation of the antagonist rule-state, and do so more rapidly when the rule-state is easier to predict. This rapid decrease in activity could underlie a process of elimination in which trajectories that do not invoke the preferred rule-state receive no further computational resources. Furthermore, discrimination between difficult and easy trials in the antagonist rule-state occurs prior to when discrimination within the agonist rule-state occurs. A winner-take-all like model that incorporates a pair of mutually inhibited integrators to accumulate evidence in favor of either the decision to pursue or the decision to continue fixation accounts for the observed neural phenomena.

Keywords Abstract rule · Accumulator model · Decision making · Primates · Smooth pursuit · Supplementary eye field

S. Ray · S. J. Heinen
The Smith-Kettlewell Eye Research Institute, San Francisco, CA, USA

S. Ray (✉)
Centre of Behavioural and Cognitive Sciences, University of Allahabad, Senate Hall Campus, Allahabad 211002, Uttar Pradesh, India
e-mail: sray@cbcs.ac.in

Introduction

While most studies of action selection have focused on how concrete rules (e.g., 'red means stop'; 'green means go') guide a one-to-one mapping between a sensory stimulus and a motor response, less is known about how abstract rules connect many sensory inputs to a specific motor output, or a specific sensory input to many motor outputs (Bunge 2004; Cisek and Kalaska 2010). For example, for the rule 'if a pedestrian is on the crosswalk then stop, but if the pedestrian is on the sidewalk then go,' pedestrians of different physical characteristics may result in a single action, and a particular pedestrian may result in different actions depending on where they are standing. The prefrontal and premotor cortices in human and non-human primates have been shown to be involved in encoding abstract rules (White and Wise 1999; Asaad et al. 2000; Wallis et al. 2001; Bunge et al. 2003; Wallis and Miller 2003; Muhammad et al. 2006; Bengtsson et al. 2009; Badre et al. 2010), which allow an arbitrary sensory motor association for limb and eye movements to be made (Mitz et al. 1991; Asaad et al. 1998).

The supplementary eye field (SEF) in the medial frontal cortex of primates (Schlag and Schlag-Rey 1987) plays a key role in conditional stimulus–response mapping for saccadic (Chen and Wise 1995, 1996) and smooth pursuit eye movements (Kim et al. 2005; Shichinohe et al. 2009). SEF

neurons of macaques have been shown to modulate activity in a conditional go–nogo task that stipulates that the animals either follow a moving target with an eye movement if it crosses a visible zone on the screen ('go'), or maintain fixation if it bypasses the zone ('nogo'). Two populations of neurons in the SEF exist, one with higher activity for the 'go' rule-state and the other with higher activity for the 'nogo' rule-state (Kim et al. 2005). These neurons are either poorly or not at all directionally tuned, and their activity signals better the veridical rule-state than the behavioral choice in the decision task (Yang et al. 2010). Furthermore, they are differentially active for the same target trajectory to signal alternative rule-states when the decision boundary is changed (Heinen et al. 2011).

SEF neurons increase activity for their preferred rule-state. We asked whether the decrease in activity of the same neurons occurring for the alternative rule-state could also play a role in decision making. We found that the activity decreased more rapidly when the non-preferred rule-state was relatively easier to anticipate, and these neurons discriminated easy trials from difficult ones in the non-preferred rule-state before they did so in the preferred rule-state. These results are consistent with the idea that activity of a neuron that decreases for the non-preferred rule-state is involved in the decision process.

We designed and simulated a computational model to understand the underlying mechanism of these neural phenomena. The model incorporates a pair of mutually inhibited integrators, each of which accumulates evidence over time in favor of a target trajectory that complies with either the 'go' or 'nogo' rule-state. The output of each integrator mimics the outputs of SEF neurons during the task.

Methods

Behavioral task

In the ocular baseball task we used, each trial began with the appearance of a white spot of diameter 0.5° visual angle, located at the center of the screen. The spot was surrounded by a visible square (12° × 12°), which we refer to as the 'plate' (Fig. 1a). To begin a trial, the monkey had to acquire fixation and maintain its gaze within a 4° electronic square window centered at the fixation point for 500 ms. At the end of the fixation period, a target that was identical to the fixation point appeared either left or right of the plate on the horizontal meridian, 20° eccentric from the center. The target then moved at a constant velocity of 30°/s toward the vertical meridian of the screen and either intersected or bypassed the plate. The direction of the trajectory was randomly selected from eight possible Cartesian angles (±10°, ±20°, ±30°, and ±40°) with respect to horizontal, yielding 16 possible trajectories. Target motion duration was 1,200 ms. The fixation point and plate remained visible throughout a trial.

The animal was required to track the target if it intersected the plate (±10° and ±20° trajectories; 'go' or 'strike' trials) using smooth pursuit eye movements, or maintain fixation if it did not (±30° and ±40° trajectories; 'nogo' or 'ball' trials), to receive liquid reward. In strike trials, the animal had to acquire the target within 300 ms after it intersected the plate and maintain gaze within 3° of it until it disappeared. The inter-trial interval ranged from 300 to 700 ms (randomly chosen). A critical aspect of ocular baseball is the delay period, which begins at the onset of target motion and extends until plate intersection. During the delay period, the animal was required to maintain fixation so that the neural activity in the absence of eye movements could be assessed.

Animal care and surgery

Two adult male rhesus (*Macaca mulatta*) monkeys weighing 7–13 kg performed the tasks. Aseptic survival surgeries were performed on each animal under Isoflurane gas anesthesia in order to implant a recording chamber over the SEF, a head-restraint device and an eye coil. A craniotomy was trephined in the skull centered at a location 24 mm anterior in Horsley–Clark stereotaxic coordinates. A stainless steel recording chamber (Crist Instrument) with an inner diameter of 1.4 cm was positioned over the craniotomy and secured along with the other implants with dental acrylic. The head-restraint device was positioned on the midline, caudal to the chamber. The eye coil was implanted under the conjunctiva of one eye. All procedures were approved by the Smith-Kettlewell Institutional Animal Care and Use Committee, in compliance with the guidelines set forth in the United States Public Health Service Guide for the Care and Use of Laboratory Animals.

Data acquisition

Experimental control and data acquisition were performed using a Pentium IV 3.4 GHz PC (Windows XP) running LabVIEW Express 7.0 (National Instruments) with the real-time module. Visual stimuli were displayed on a 24″ computer monitor driven by a Macintosh G4 (MacOS 9) system, using MATLAB (The MathWorks, Inc.) software and the Psychophysics Toolbox real-time visual display tools (Brainard 1997). Eye position signals were recorded using a magnetic field system (CNC systems) or a video-based eye tracker (EyeLink 1000). Horizontal and vertical eye velocities were calculated off-line by differentiating and filtering the recorded eye position signals, using a 2-pole Butterworth non-causal filter with a cutoff of 50 Hz.

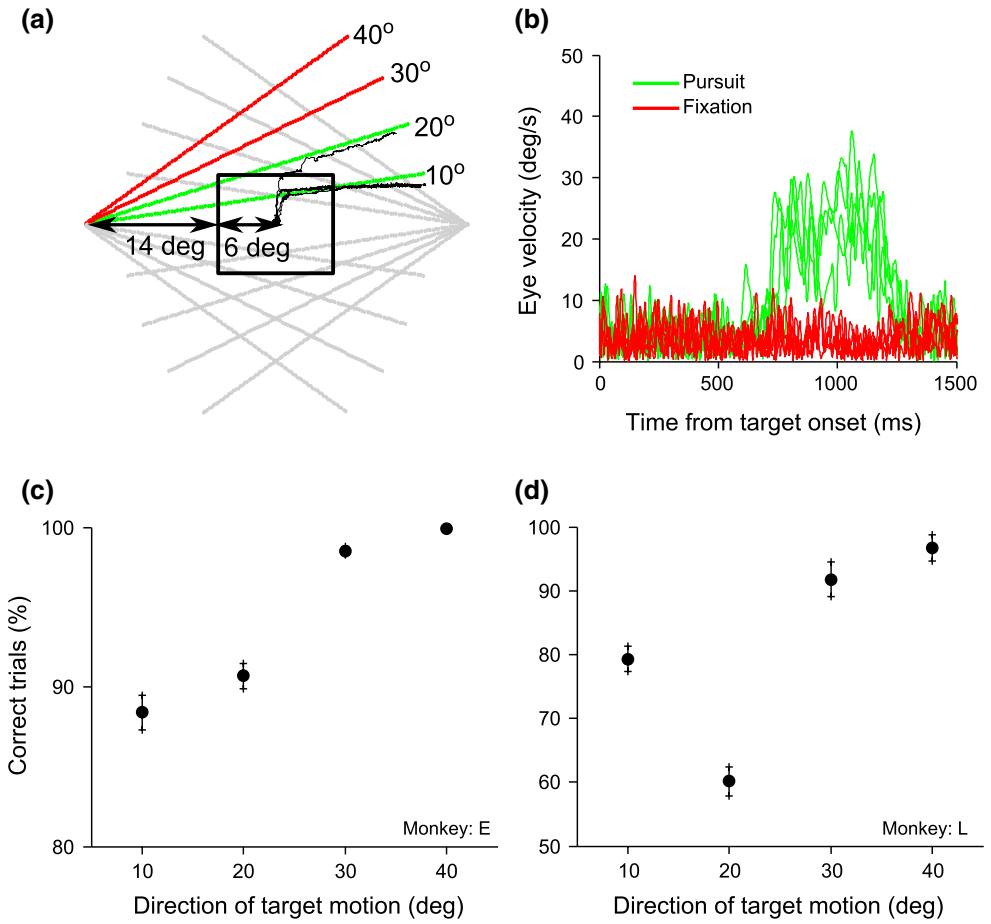

Fig. 1 **a** Oculomotor baseball task. The target appeared either left or right to a square (*plate*) and moved toward the vertical meridian of the screen along one of sixteen straight trajectories that subtended 10°, 20°, 30°, and 40° relative to the horizontal meridian. The animal tracked the target using smooth pursuit eye movements (gaze traces shown by *thin black lines*) after it intersected the plate in 'strike' trials (*green lines*: 10° and 20°) or maintained fixation if it did not in 'ball' trials (*red lines*: 30° and 40°). **b** Eye velocity in strike (*green*) and ball (*red*) trials. **c**, **d** Performance of individual animals in the task for each motion directions

The computer acquired the eye position signals at a sampling rate of 1.0 kHz. Single neurons were recorded from the SEF using tungsten microelectrodes (FHC) with an impedance of 1.0–3.0 MΩ, tested at 1,000 Hz. A manual hydraulic (Trent Wells Inc.) or a motorized (Crist Instrument) microdrive was used to advance the microelectrode through the recording chamber. Electrical signals from the electrode were fed into a TDT Medusa preamplifier (Tucker Davis Technologies, Alachua, FL). Amplified signals were sampled at 25 kHz, and spikes were isolated by TDT OpenEx software with high- and low-pass filters at 6 kHz and 500 Hz, respectively.

Data analysis

All data analyses were conducted off-line using custom-made programs written in MATLAB (The MathWorks, Inc.). The raw spike counts were converted into a continuous smoothed spike density function aligned on target onset by convolving a Gaussian function having a fixed temporal width of 20 ms. To determine the time that neuronal activity first became different for strike and ball trials, we subtracted the spike density function averaged across strike trials from the spike density function averaged across ball trials for each neuron. The absolute value of the resulting spike density function will be referred to as the differential spike density function. The time at which significant differential activity between strike and ball trials began was defined as the instant at which the difference in post-target spike density exceeded twice the standard deviation (2SD) of the mean absolute difference in activity in a 300-ms interval prior to target presentation, provided that the difference eventually reached four times the standard deviation (4SD) and remained above the 2SD threshold for at least 50 ms (Ray et al. 2009). Pre-target differential activity was used to set the threshold in order to minimize the chance

of false identification of task-unrelated post-target differential activity. Our criterion for determining whether a given neuron discriminated between rule-states was that the onset of significant differential activity occurred between 80 ms (visual delay in the SEF, Pouget et al. 2005) and the average pursuit onset time (see Fig. 2a–d). Only those neurons that discriminated between rule-states were used for further analysis in the manuscript.

The ability of populations of neurons to discriminate two different target trajectories within a rule-state (either 'go' or 'nogo') was examined using receiver operating characteristic (ROC) analysis (Green and Swets 1966). Rewarded trials were sorted by target trajectory angle. Neurons that contributed at least ten trials corresponding to each of the four angles of target trajectories were included in the analysis. The spike density functions within a rule-state accompanying a pair of angles in which the animal either tracked the target (strike trials: ±10° and ±20°) or maintained fixation (ball trials: ±30° and ±40°) were compared. We grouped all correct trials into four sets corresponding to four cardinal motion directions with respect to the horizontal meridian irrespective of sign, i.e., 10°, 20°, 30°, and 40°. Spike trains from each of the original set of trials were resampled to construct 500 sets of simulated spike trains for a reliable comparison (Song and McPeek 2010). In each of these resampled sets, the number of simulated spike trains was the same as the number of original spike trains. A simulated spike train was constructed by randomly selecting one trial from the set of original trials at every 1 ms. If a spike occurred in that trial at that instant, the spike was added to the simulated spike train. Spike density functions were constructed for these spike trains by aligning them on the time of target onset and convolving a Gaussian function having a fixed temporal width of 20 ms. The proportion of trials exhibiting a higher firing rate than a criterion in one set was plotted against that for the other set at a given time to construct a ROC curve by varying the criterion from zero to the maximum firing rate at a regular interval of 1 spike/s. Comparisons were conducted by calculating the areas under the ROC curves for successive 1-ms increments, starting 200 ms before target presentation and continuing for the next 1,200 ms. The area under the ROC curve provides a quantitative measure of the separation between two distributions of activity. An area under the ROC curve of 0.50 signifies that the two distributions are completely overlapping, whereas the extreme values of 0.00 or 1.00 signify that the two distributions are completely non-overlapping.

Model description

In order to examine the mechanism underlying discrimination of decision rules by two complementary populations of SEF neurons, we designed a computational framework that primarily consists of a comparator and a pair of mutually inhibited leaky integrators (Fig. 4a). The following are the key assumptions underlying the model. (1) A comparator estimates the vertical distance between the target and a noisy representation of an imaginary straight line that connects the origin of the target and the corner of the plate nearest to the target trajectory. We refer to this line as the decision boundary, since this line divides target trajectories into two groups corresponding to alternative motor decisions: ocular pursuit and fixation. (2) At time t of the simulation, the location (x, y) of the moving target in a two-dimensional Cartesian coordinate system is calculated from $x = -\text{ecc} + vt\ \cos\theta$ and $y = vt\ \sin\theta$, where ecc is the eccentricity (=20°), v is the velocity (30°/s), and θ (10°/20°/30°/40°) is the angular direction of the target. (3) The vertical position of the decision boundary at a time t is $y_B = vt\ \cos\theta\ \tan\beta + \Delta y_B$, where β (=23.2°) is the inclination of the decision boundary on the horizontal meridian and Δy_B is a random number sampled from white Gaussian noise of power ρ. (4) If the position of the target lies on or below the decision boundary (i.e., $y \leq y_B$), the comparator signals that the target is likely to intersect the plate, and if the position of the target lies above the boundary (i.e., $y > y_B$), the comparator signals that the target is likely to miss the plate. Therefore, at a given instance of time, the comparator enables either the GO or NOGO unit to sample evidence. (5) At each clock tick, either the GO or NOGO unit samples evidence in favor of either ocular pursuit or fixation, respectively, from a normal distribution. The new sampled evidence is then added to the total evidence gathered up to that point of time in the corresponding integrator. (6) Information leaks from each integrator in proportion to the amount of evidence gathered by that integrator. (7) The GO and NOGO units inhibit each other with strength proportional to the amount of evidence available in the individual integrators. Note that without inhibition, a loss of evidence already accumulated could balance the accumulation of new evidence, resulting in the net evidence accumulated by the GO and NOGO units reaching asymptotic levels (Usher and McClelland 2001). (8) Because the firing rate of a neural population is finite and limited, an additional dissipation of information begins as soon as the accumulated evidence reaches a threshold (=1) at a rate proportional to the amount of evidence available in the corresponding integrator.

In practice, at every 1-ms interval, net evidence in the GO (u_{GO}) and NOGO (u_{NOGO}) units was increased by Δu_{GO} and Δu_{NOGO}, respectively. If the GO unit was enabled to sample new evidence, $\Delta u_{GO} = I_{GO} - \gamma u_{GO} - \eta u_{NOGO} - \phi u_{GO}$ and $\Delta u_{NOGO} = 0$; if the NOGO unit was enabled, $\Delta u_{NOGO} = I_{NOGO} - \gamma u_{NOGO} - \eta u_{GO} - \phi u_{NOGO}$ and $\Delta u_{GO} = 0$, where I was input (evidence) to either GO or NOGO unit sampled from a Gaussian distribution with

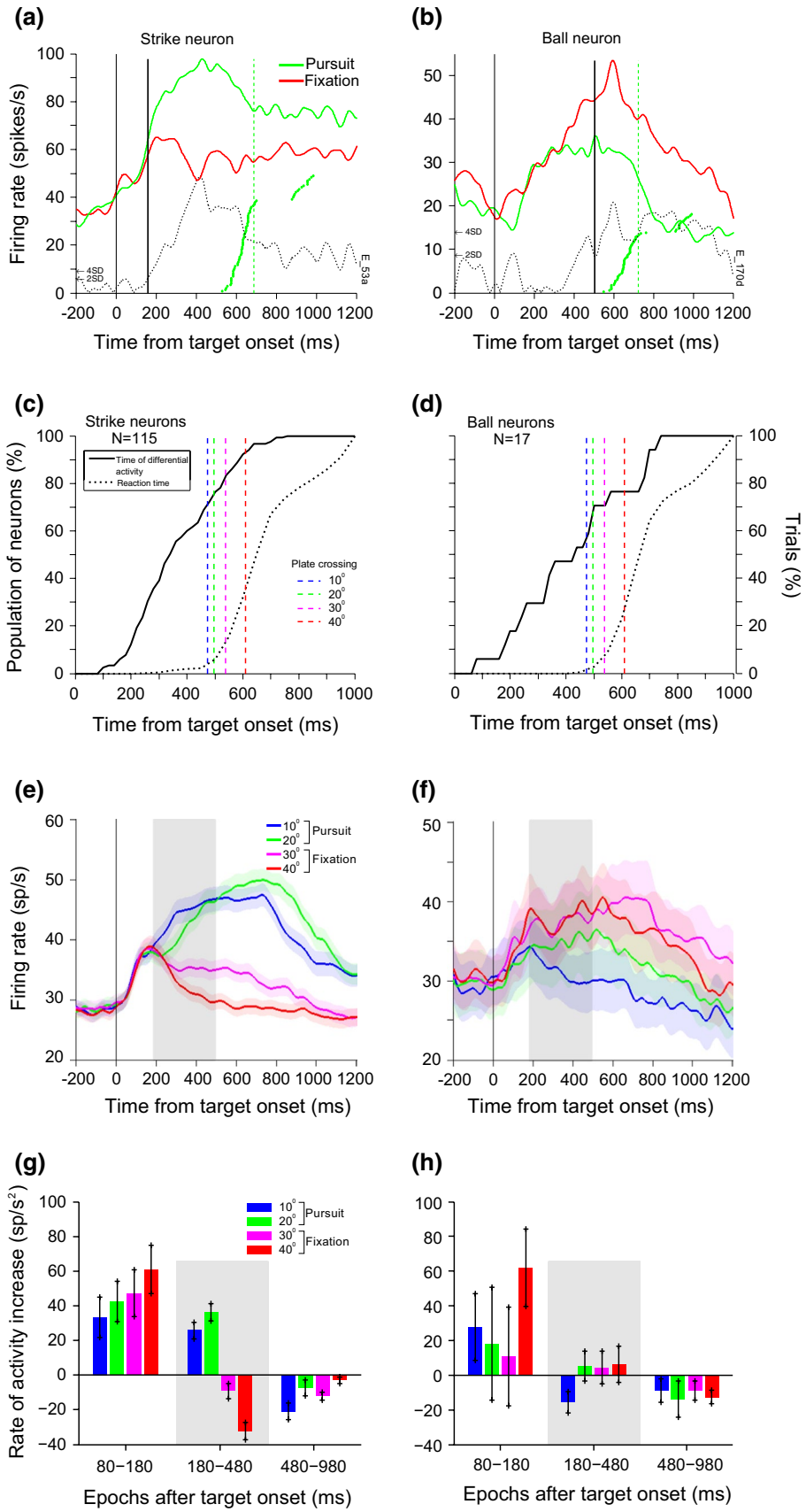

Fig. 2 Activity of a representative *strike* neuron (**a**) and a *ball* neuron (**b**) in the SEF during pursuit ('go' rule-state, green traces) and fixation ('nogo' rule-state, red traces) aligned on the target onset. Neurons increased or decreased activity to indicate their preferred or non-preferred rule-state, respectively. *Thick black lines* demarcate the time of significant differential activity shown by *dotted black lines*. *Green dots* indicate pursuit latencies in individual strike trials on the abscissa. *Broken green lines* indicate the average pursuit latencies. Cumulative distributions of the time of differential activity between pursuit and fixation for the populations of strike (**c**) and ball (**d**) neurons are shown by *solid black lines*. Pursuit latency distributions across trials in the corresponding sessions are shown by *black dotted lines*. *Broken blue and green lines* indicate delays to intersect the plate when the target moved along 10° and 20° trajectories. *Broken magenta and red lines* indicate delays to intersect an imaginary vertical extension of the leading edge of the plate when the target moved along 30° and 40° trajectories. Neural discrimination of go–nogo rule-states was mostly predictive as it happened before the stimulus fulfilled the condition for a rule-state. Spike density functions averaged across the populations of strike (**e**) and ball (**f**) neurons when the target moved along 10° (*blue*), 20° (*green*), 30° (*magenta*), or 40° (*red*) trajectories. *Shaded regions* of corresponding *colors* indicate standard error of the mean. The average (±s.e.m) rate of increase in activity of strike (**g**) and ball (**h**) neurons in three consecutive epochs after the target onset was different for different motion directions. Both types of neurons exhibited a rapid decrease in activity in the second epoch (highlighted by *gray rectangles*) when their non-preferred rule-state was easier to anticipate

mean μ and standard deviation σ. The strengths of leakage and inhibition were γ and η, respectively. The strength of dissipation (φ) in addition to leakage remained at 0 until the accumulated evidence u_{GO} or u_{NOGO} reached the threshold (=1).

Estimation of model parameters

Because discharge rate of strike neurons in response to 10° motion direction peaked on average (±s.e.m) 506 ± 29 ms after target onset, we estimated the mean ($\mu = 0.002$ ms^{-1}) and arbitrarily chosen the standard deviation ($\sigma = 0.01$ ms^{-1}) of the distribution from which $I_{GO/NOGO}$ was sampled. We set the power (ρ) of the 'band-limited white noise' simulation block to 20 to introduce noise on the decision boundary (for further reference, see www.mathworks.com/help/simulink/slref/bandlimitedwhitenoise.html). The strengths of leakage (γ), supra-threshold dissipation (φ), and the strength of inhibition (η) were optimized to 0.0005, 0.008, and 0.002, respectively. This was done by minimizing the difference between the time of neural discrimination between alternative rule-states (i.e., 'go' vs. 'nogo') and the time when the difference between evidence accumulated by the GO and NOGO units exceeded a discrimination threshold (=0.47), in response to 10° motion direction. This discrimination threshold was calculated from the average normalized differential activity in two populations of SEF neurons (Fig. 3c). Optimization was performed using the 'Least Square' method in the 'Parameter Estimation' toolbox for Simulink (MathWorks, Inc.) during simulation of a set of 144 trials. The set size was equal to the number of data points shown in Fig. 3c.

Results

In our go–nogo 'ocular baseball' task, monkeys either tracked a moving target with a pursuit eye movement after the target intersected a visible square (plate) in 'strike' trials or maintained fixation if it did not in 'ball' trials (Fig. 1a, b). Performances of the animals E and L are shown in Fig. 1c, d, respectively. In each recording session for motion directions 10°, 20°, 30°, and 40°, monkey E was rewarded in on average (±s.e.m) 88.4 (±1.08), 90.7 (±0.81), 98.5 (±0.26), and 99.9 (±0.05) percent of trials, and monkey L was rewarded in on average (±s.e.m) 79.3 (±2.0), 60.1 (±2.27), 91.8 (±2.71), and 96.7 (±2.06) percent, respectively. A nonparametric Kruskal–Wallis test for equal medians of samples in multiple groups showed that the proportion of correct trials varied across motion directions for each animal ($P < 0.001$); however, a t test suggested that monkey E's performance was not different between the angles of trajectories in strike trials.

We distinguished two types of neurons in the SEF. One population exhibited a higher firing rate when the target intersected the plate in strike trials relative to when it bypassed the plate in ball trials. We refer to these neurons as *strike* neurons. Another population, to which we refer as *ball* neurons, exhibited higher firing rate when the target bypassed the plate. In this study, we recorded 163 strike and 34 ball neurons. Among them, a total of 132 neurons (strike: 115, ball: 17) that fulfilled the criterion of having significantly differential activity in rewarded trials was considered for analyses throughout (see "Methods"). Paired t test showed that the average (±s.e.m) firing rate of strike neurons aligned on the target onset in strike trials was 41.5 ± 1.5 spikes/s during target motion, which was significantly ($P < 0.001$) higher than the average (±s.e.m) firing rate of 31.6 ± 1.3 spikes/s in ball trials during the same period. Similarly, the average (±s.e.m) firing rate of ball neurons in ball trials was 35.9 ± 4.0 spikes/s, which was significantly ($P < 0.001$) higher than the average (±s.e.m) firing rate of 30.6 ± 3.6 spikes/s in strike trials.

Activity of representative strike and ball neurons is shown, respectively, in Fig. 2a, b for correct strike and ball trials. Vertical thick black lines demarcate the times at which the differential activity traces, shown by dotted black lines, reached a significant level (see "Methods"). Figure 2c, d shows the cumulative distributions of the time of differential activity (solid back) across populations of strike and ball neurons, respectively, and the cumulative distributions of reaction times (dotted black) across trials in the corresponding sessions. Vertical broken lines show the delays at which the target either intersected the vertical leading edge of the plate when moved along 10° (blue) or 20° (green) trajectories in strike trials, or intersected an imaginary extension of that when moved along 30° (magenta) or 40° (red) trajectories in ball trials. Note that the majority of neurons in each population exhibited increase in activity before the stimulus physically satisfied the condition of the preferred rule-state. In 10.6 % go trials, eye movement began either just before the target intersected the plate or within the visual latency of 80 ms in the SEF after the intersection, with the mean (±SD) delay of 47 ± 26 ms. Strike neurons distinguished between go and nogo rule-states on average (±s.e.m) 382 ± 14 ms after the target onset, which was significantly ($P < 0.001$) earlier than the average (±s.e.m) 711 ± 2 ms pursuit latency, and ball neurons distinguished between rule-states on average (±s.e.m) 430 ± 49 ms following the target onset, which was significantly ($P < 0.001$) earlier than the average (±s.e.m) 728 ± 4 ms pursuit latency. Together, these results suggested that the SEF distinguished between go and nogo rule-states before the corresponding condition was fulfilled, and in some go trials, the predictive rule discrimination resulted in faster eye movements around the time when the target intersected the plate.

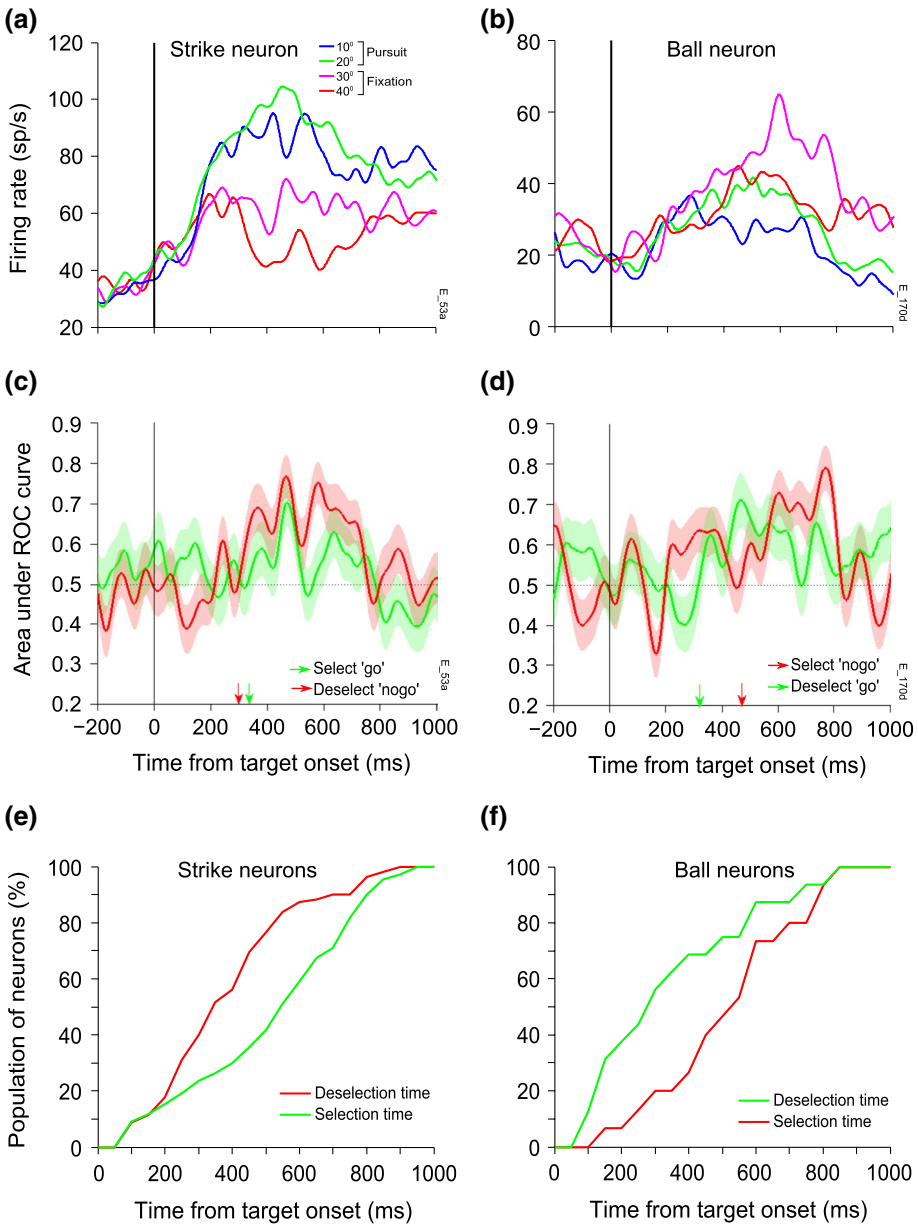

Fig. 3 Spike density functions of the representative strike (**a**) and ball (**b**) neurons when the target moved along 10° (*blue*), 20° (*green*), 30° (*magenta*), or 40° (*red*) trajectories. Discrimination of target trajectories within a rule-state obtained from a ROC analysis for the representative strike (**c**) and ball (**d**) neurons in (**a**) and (**b**). Area under the ROC curve (AUC) was calculated by comparing the activity of a neuron for two different motion directions specifying the same rule-state. *Line trace* shows AUC averaged over 500 resampled sets of spike trains. *Shaded region* indicates standard deviation of the mean. Comparison between motion directions in go and nogo rule-states is shown by *green* and *red traces,* respectively. The selection time and the deselection time were calculated when the corresponding average AUC significantly ($P < 0.05$) grew above 0.50 to reach its maximum. The strike neuron deselected the antagonist (nogo) rule-state, i.e., discriminated easy (40°) from difficult (30°) ball trials (*red arrow*), earlier than it selected the agonist (go) rule-state, i.e., discriminated easy (10°) from difficult (20°) strike trials (*green arrow*). Similarly, the ball neuron deselected the antagonist (go) rule-state (*green arrow*), earlier than it selected the agonist (nogo) one (*red arrow*). Cumulative distributions of selection and deselection times of agonist and antagonist rule-states over the strike (**e**) and ball (**f**) neuron populations

Both populations of neurons initially increased activity up to an intermediate level irrespective of the motion direction, following which they either further increased activity for the preferred rule-state or decreased activity for the non-preferred rule-state. We sought to know whether SEF neurons simply discriminate rule-states by separating motion directions into two sets, one that satisfies a preferred stimulus condition and the other that does not,

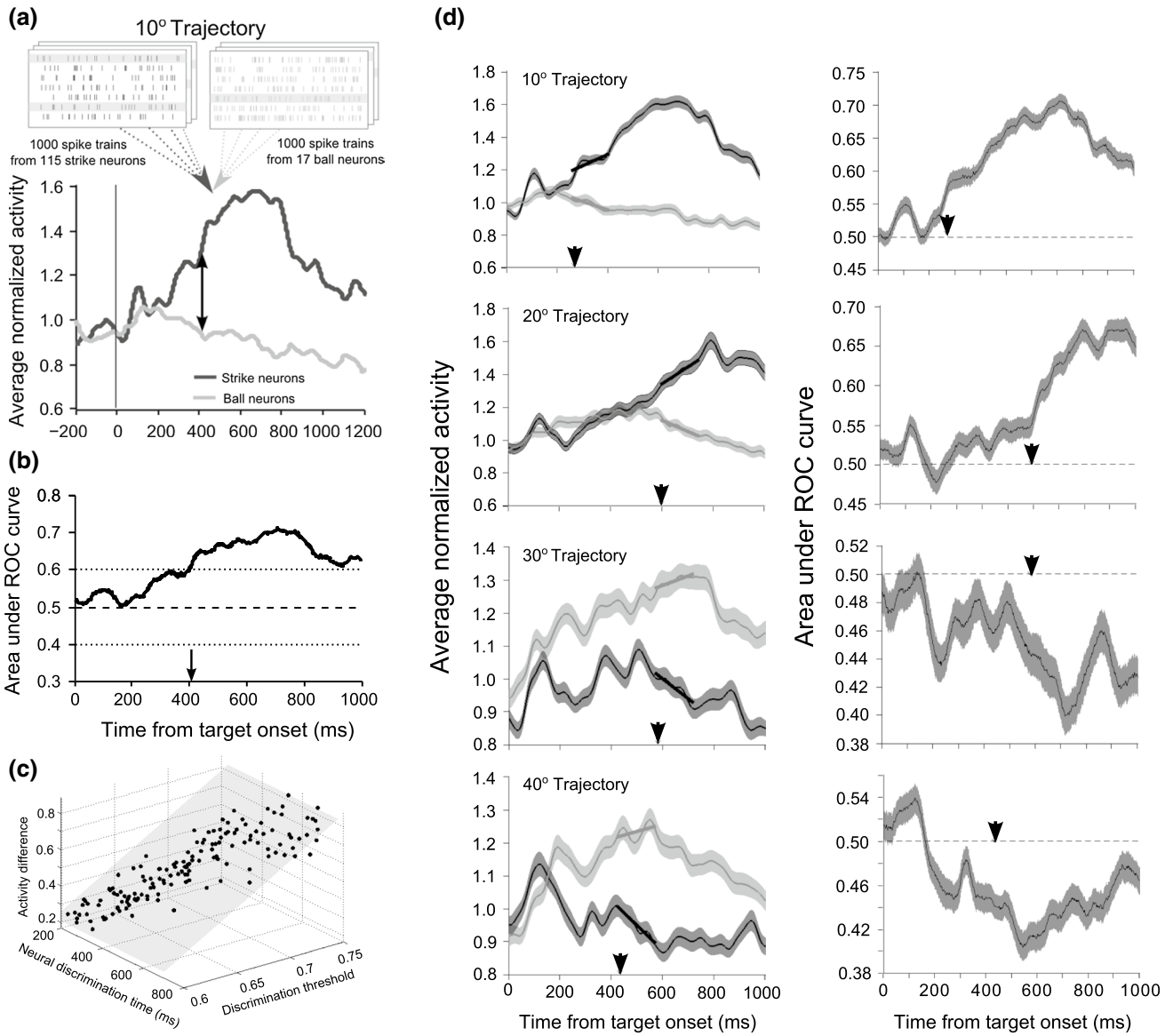

Fig. 4 Neuron–antineuron analysis of rule discrimination that simulates simultaneous recording of all neurons in both strike and ball populations. **a** One or more correct trials were arbitrarily chosen from each recording session to construct a set of 1,000 spike trains for each type of SEF neuron. Mean spike density functions for strike (*black*) and ball (*gray*) neurons were normalized separately and averaged over a period of 300 ms prior to the target appearance. **b** ROC analysis to compare distributions of spikes generated by the two populations of neurons in response to 10° trajectories. Area under the ROC curve (AUC) plotted as a function of time shows the dynamics of the difference between strike and ball activity in response to the motion direction. *Dotted lines* indicate thresholds (0.5 ± 0.1) for discrimination. The *arrow head* denotes the time when the AUC reaches a threshold and neurons signal their preferred rule-state. A *bidirectional arrow* in (**a**) indicates the difference between normalized activity of strike and ball neurons at that time. **c** Normalized differential activity plotted as a function of AUC threshold and the time when AUC reached the threshold. The *shaded region* shows a surface fit of data points, which steadily increased with threshold. **d** Normalized average (±s.e.m) spike density functions (*left panel*) and corresponding average (±s.e.m) AUC function (*right panel*) for 10°, 20°, 30°, and 40° trajectories are shown from *top* to *bottom* in order. Linear regression fits are overlaid on spike density functions. Other conventions are same as in (**a**) and (**b**). Note that rule-state discrimination occurred earlier in easy trials, and while one type of neurons increased activity, other type decreased in a critical period when they resolved the rule-state

or distinguish between motion directions within a set as well. If the former is the case, the dynamics of modulation in the SEF activity for two different motion directions in the same rule-state should be the same; and if the latter, the two different motion directions within the same rule-state should modulate the activity differently. To this end, we grouped all correct trials into four mutually exclusive cardinal sets. Target trajectories in each set of trials subtended

the same angle with respect to the horizontal meridian irrespective of sign, i.e., 10°, 20°, 30°, and 40°. In strike trials, the motion directions (10° and 20°) specify the go rule-state, which is the agonist rule-state for strike neurons but the antagonist rule-state for ball neurons. In ball trials, the motion directions (30° and 40°) specify the nogo rule-state, which is the agonist rule-state for ball neurons but the antagonist rule-state for strike neurons. The average (±s.e.m) spike density functions across the population of strike and ball neurons are shown, respectively, in Fig. 2e, f for each cardinal set trajectory.

Paired *t* tests showed that the average (±s.e.m) firing rate (42. 1 ± 1.5 spikes/s) of strike neurons during target motion along 20° was significantly ($P < 0.05$) higher than that during motion along 10° (40.9 ± 1.6 spikes/s), and the average (±s.e.m) firing rate (32.9 ± 1.4 spikes/s) for 30° trajectories was significantly ($P < 0.05$) higher than that for 40° trajectories (30.3 ± 1.2 spikes/s). The same analysis showed that the average (±s.e.m) firing rate (32.0 ± 3.9 spikes/s) of ball neurons for 20° trajectories was significantly ($P < 0.05$) higher than that for 10° trajectories (29.2 ± 3.4 spikes/s). Although the average (±s.e.m) firing rate of ball neurons for 30° trajectories (36.5 ± 3.9 spikes/s) was higher than that for 40° trajectories (35.2 ± 4.2 spikes/s), and the majority (59 %) of ball neurons exhibited higher firing rate for 30° trajectories than 40° trajectories, the difference was not statistically significant ($P = 0.15$). We speculate that ball neurons performed poorly in the statistical test due to small sample size.

If indeed SEF neurons distinguish between motion directions within a rule-state, not only the average firing rates, but also the dynamics of modulation of activity should also be different for different motion directions. We calculated the rate of change in the firing rate of individual neurons from linear regression fit of the spike density function in three consecutive epochs of duration 100, 300, and 500 ms starting from 80 ms after target onset, which is the visual delay in the SEF (Pouget et al. 2005). Durations of epochs were selected based on the observation that the activity of both types of neurons increased for first ~200 ms after the target onset, following which the agonist activity increased for ~300 ms before decreasing subsequently (for example, see the representative neurons in Fig. 2a, b). The average (±s.e.m) rates of change in firing rate of strike and ball neurons are shown, respectively, in Fig. 2g, h.

First, we focus on the second epoch (highlighted), i.e., from 180 to 480 ms after target onset, because this is the most important epoch in relation to predictive rule discrimination. In this epoch, the average (±s.e.m) rate of increase in strike activity for 20° trajectory (36 ± 5 spikes/s^2) was significantly ($P < 0.05$) higher than 10° trajectory (26 ± 5 spikes/s^2), and the average (±s.e.m) rate of decrease was significantly ($P < 0.001$) higher for 40° (−32 ± 5 spikes/s^2) than 30° trajectories (−9 ± 4 spikes/s^2). In the same epoch, ball neurons increased activity for 40° trajectories at the same rate as for 30° ones, but decreased activity for 10° trajectories (−16 ± 6 spikes/s^2) significantly ($P < 0.05$) faster than 20° trajectory (5 ± 8 spikes/s^2). This result indicates that in both populations of neurons, activity decreased at a faster rate when the non-preferred rule-state was easier to resolve. The rates of increase in activity for motion directions within the go (i.e., 10° and 20° trajectories) and nogo (i.e., 30° and 40° trajectories) rule-states were not statistically different in the first epoch for both types of neurons. In the third epoch, activity of strike neurons for 10° (−21 ± 5 spikes/s^2) and 30° (−12 ± 2 spikes/s^2) trajectories decreased at significantly ($P < 0.001$) higher rates than 20° (−7 ± 5 spikes/s^2) and 40° trajectories (−3 ± 2 spikes/s^2), respectively. The rate of decrease in activity of ball neurons in this epoch was the same for motion directions specifying the go and nogo rule-sates.

We sought to determine why neurons exhibited lower activity for trajectories within a rule-state that were farther away from the nearest corner of the plate in the direction of target motion (Fig. 2e, f). For instance, both strike and ball neurons exhibited lower activity when the target moved along 10° trajectories than when it moved along 20° trajectories. We hypothesized that SEF neurons exhibited lower discharge rate when a trajectory was farther from the imaginary decision boundary connecting the origin of the target and nearest corner of the plate, making the rule-state easier to resolve. It would make sense to turn off neurons earlier when a rule-state was identified so that the computational resources could be conserved. We next sought to determine whether SEF neurons discriminated easy from difficult trials within the same rule-state, and if so, at what time the discrimination occurred. To obtain an unbiased estimate of the difference in activity for different trajectories within a rule-state, we used a nonparametric receiver operating characteristic (ROC) procedure based on signal detection theory (Green and Swets 1966; MacMillan and Creelman 1991). Our method was adapted from previous works using ROC analysis to determine differences in neural activity (e.g., Britten et al. 1992; Krauzlis and Dill 2002; Song and McPeek 2010). We calculated the area under the ROC curve (AUC) at each millisecond to derive an AUC function. Each neuron yielded two AUC functions, one for the go rule-state and another for the nogo rule-state, from four sets of trials corresponding to the four motion directions (see "Methods"). Three criteria had to be met to establish when a neuron first discriminated two motion directions within a rule-state: (1) the average AUC grew significantly (one-tailed *t* test, $P < 0.05$) above the 0.5 level, (2) remained significantly above the 0.5 level for at least 50 ms, and (3) it continued to grow to the maximum without returning at the 0.5 level. We refer to the earliest time

of discrimination between motion directions within the preferred rule-state as the *selection time.* If the discrimination was between motion directions within the non-preferred rule-state, we refer to the earliest time of discrimination as the *deselection time*.

Figure 3a, b shows spike density functions of representative strike and ball neurons, respectively, for different motion directions. Figure 3c, d shows the average AUC across 500 iterations plotted as a function of time for the same neurons (see "Methods" for the bootstrapping technique). Green and red traces plot the average AUC functions for a neuron's activity in difficult trials and were compared to that in easy trials within the go and nogo rule-states, respectively. Shading indicates standard deviations of the corresponding AUC functions. The deselection of the non-preferred or antagonist (nogo) rule-state and the selection of the preferred or agonist (go) rule-state by the strike neuron in Fig. 3a occurred 297 ms and 336 ms after target onset, respectively (Fig. 3c). The ball neuron in Fig. 3b deselected the antagonist (go) rule-state and selected the agonist (nogo) rule-state 318 ms and 465 ms after target onset, respectively (Fig. 3d).

Figure 3e, f shows cumulative distributions of selection and deselection times in the populations of strike and ball neurons. For strike neurons, 110 neurons selected the go rule-state and 112 neurons deselected the nogo rule-state. The average (±s.e.m) deselection time (399 ± 19 ms) across the population was significantly ($P < 0.001$) earlier than the selection time (535 ± 23 ms). For 107 strike neurons that both deselected the nogo rule-state and selected the go rule-state, the average (±s.e.m) deselection time (400 ± 20 ms) was significantly earlier than the average (±s.e.m) selection time (534 ± 23 ms) (paired t test, $P < 0.001$). In the population of ball neurons, 15 neurons selected the nogo rule-state and 16 neurons deselected the go rule-state. The average (±s.e.m) deselection time (356 ± 61 ms) across the population of ball neurons was significantly ($P < 0.05$) earlier than the selection time (539 ± 53 ms). However, for 14 ball neurons that both deselected the go rule-state and selected the nogo rule-state, while the average (±s.e.m) deselection time (377 ± 68 ms) was earlier than the selection time (528 ± 55 ms), the difference was not statistically significant (paired t test, $P = 0.058$), possibly due to small size of this population.

Note that the animals had to refrain from making an ocular pursuit movement until the target intersected the plate. Therefore, a neuron could discriminate between go and nogo rule-states by merely monitoring whether the target physically contacted the plate. To rule out this possibility, we compared the earliest time that a target intersected or bypassed the plate with the average selection and deselection times of the population. The earliest time that the target met the go criterion was 474 ms, which was the plate intersection time of the 10° trajectory. The earliest time that the target met the nogo criterion was 539 ms, which was the time at which it crossed an imaginary extension of the leading vertical edge of the plate when moving along a 30° trajectory. These times were much later than the average deselection times (go rule-state: 399 ms, nogo rule-state: 356 ms) ($P < 0.05$), but not later than the average selection times (go rule-state: 534 ms, nogo rule-state: 539 ms). These findings suggest that SEF neurons discriminated between go and nogo rule-states by predictively decreasing activity to deselect the antagonist rule-state.

We asked whether a winner-take-all (WTA) interaction between strike and ball neurons in the SEF could account for the predictive antagonist rule deselection we observed. Under this mechanism, one type of SEF neurons increase activity to signal its preferred rule-state, while the other type decreases activity to signal that its preferred rule-state will not occur. We used a 'neuron–antineuron' analysis to deduce how the population of strike and ball neurons would have responded to a given motion direction if we recorded from all sampled neurons in each category simultaneously (e.g., Krauzlis and Dill 2002). The analysis was based on two sets of spike trains corresponding to strike and ball populations of neurons generated by arbitrarily sampling at least one trial from each recording session. One or more correct trials were chosen randomly from each recording session and used to construct two sets of 1,000 spike trains, one corresponding to the population of strike and the other corresponding to the population of ball neurons, for each motion direction. Spike density functions were computed for each set of spike trains by convolving the average spike count in every 1-ms bin with a Gaussian kernel ($\sigma = 20$ ms).

Figure 4a shows the spike density function for the 10° trajectory normalized to the average spike density 300 ms prior to target onset. Figure 4b shows the AUC function obtained from spike density functions in Fig. 4a, indicating the dynamics of discrimination of the go from the nogo rule-states by two populations of SEF neurons. The down arrow in Fig. 4b shows that 401 ms after the target onset, the AUC reached a critical threshold, which we arbitrarily set at 0.60 for illustration (Krauzlis and Dill 2002), and the bidirectional arrow in Fig. 4a shows that the difference between normalized strike and ball activity was 0.32 at that time. We repeated this 'neuron–antineuron' analysis for 150 AUC threshold values ranging between 0.60 and 0.75 at an interval of 0.001, and plotted the difference between normalized strike and ball activity as a function of both time and threshold (Fig. 4c). The steady rise of the surface that fits the data derived from this analysis along the z-axis (goodness of fit: $R^2 = 0.9$) indicates that two complementary populations of SEF neurons continued to discriminate between go and nogo rule-states between ~200 and 800 ms

Table 1 Neural discrimination time (NDT), i.e., the earliest time when strike and ball neurons exhibited complementary activity in response to a motion direction, and the rate of change in activity in a 150-ms window after NDT, for each motion direction

Trajectory (°)	NDT (ms)	Slope (ms^{-1})	
		Strike	Ball
10	256	0.0007	−0.0005
20	595	0.0010	−0.0007
30	569	−0.0006	0.0003
40	422	−0.0008	0.0002

irrespective of the criterion threshold. The data shown in Fig. 4c were used to optimize a computational model of decision rule discrimination, which is described in the following paragraph (also see "Methods").

In order to determine the time of neural discrimination, we (1) randomly sampled spike trains from both strike and ball neurons to generate two sets of one thousand trials each for a given direction of motion; (2) performed ROC analysis (see "Methods") on these sets of spike trains aligned at the target onset and generated an AUC function; (3) repeated this procedure one hundred times and calculated the average AUC; and (4) performed a *t* test at every millisecond to determine whether the average AUC at that instant significantly ($P < 0.05$) increased above (or decreased below) 0.5. Subsequently, three criteria had to be met to determine the earliest time when two types of the SEF neurons discriminated a motion direction: (1) the average AUC grew (or reduced) significantly ($P < 0.05$) above (or below) the 0.5 level, (2) remained significantly above (or below) the 0.5 level for at least 50 ms, and (3) it continued to grow to the maximum (or reduced to the minimum) without returning at the 0.5 level. The spike density function and the corresponding AUC function for each motion direction are shown in Fig. 4d. We also measured the rate of change in the normalized average activity of both populations of neurons from slopes of linear regression fits over the 150 ms after the corresponding AUC function reached the discrimination threshold (thick straight lines in Fig. 4d). Results from this analysis are summarized in Table 1. Note that the differential activity exhibited by strike and ball neurons occurred earlier in easier trials, and when one type of neurons increased activity to select a rule-state, the other types of neurons deselected the rule-state by decreasing activity.

Given that the complementary activity of strike and ball neurons suggests a WTA interaction between these populations, we designed a computational model consisting of a pair of integrators, one subserving the go rule-state and the other subserving the nogo rule-state (Fig. 5a, also see "Methods"). The integration occurs via a positive feedback connection on each unit, and the integrators are coupled by mutual inhibition in a WTA fashion (e.g., Roxin and Ledberg 2008; Oster et al. 2009). On each iteration, the model compares the vertical distance between the location of the moving target and a noisy representation of the decision boundary. In the absence of noise, the decision boundary is an imaginary line that connects the target's initial position to the corner of the plate in the direction of target motion and remains either above the trajectory in strike trials, or below the trajectory in ball trials. The comparison yields a 'vote' of whether the target will bypass (nogo rule-state) or intersect (go rule-state) the plate, which enables either the NOGO or the GO integrator, respectively, to sample and accumulate evidence. At any instant, the integrators dissipate information and inhibit each other with strength proportional to the amount of evidence accumulated up to that point in time. We first optimized our model using neural data obtained from only the 10° trajectories (Fig. 4c) and then simulated 500 trials each for all four cardinal directions. Figure 5b shows the average (±s.e.m) activity in GO (green) and NOGO (red) integrators over the simulated trials for the four cardinal motion trajectories (upper panel) and the corresponding AUCs (lower panel). For strike trials, the AUC rose more rapidly from 0.5 for the 10° trajectory than for the 20° trajectory, and in ball trials, it fell more rapidly from 0.5 for the 40° trajectory than the 30° trajectory, mimicking the AUC functions obtained from the neural data (Fig. 4b, d, right column).

The average (±s.e.m) GO (left) and NOGO (right) activity across 500 simulated trials for each of the four cardinal motion directions is shown in Fig. 6a. We further tested whether the model could explain the faster decrease in the GO and NOGO activity in easier trials that invoked the antagonist rule-state with greater certainty. To this end, we measured the rate of change in the output of the accumulators in three consecutive epochs in the same way that we measured the rate of change in the neural data, an epoch corresponding to the first 200 ms after the target onset, followed by subsequent 400 and 600 ms ones. These epochs were chosen based on the observation that in the first epoch, accumulators do not discriminates rule-states; in the second, the difference in the outputs of the accumulators reaches maximum; and in the last, outputs from both accumulators decrease. In the second epoch, the critical epoch for predictive rule discrimination of the neurons, the average (±s.e.m) activity in the GO unit corresponding to 40° trajectories (-0.42 ± 0.01 s^{-1}) decreased at a faster rate than 30° trajectories (-0.05 ± 0.02 s^{-1})($P < 0.001$) (Fig. 6b, left). The average (±s.e.m) activity in the NOGO unit corresponding to 10° trajectories decreased at a greater rate (-0.32 ± 0.01 s^{-1}) than for the 20° trajectories, which increased in rate slightly (0.23 ± 0.01 s^{-1})($P < 0.001$) (Fig. 6b, right). Both GO and NOGO units showed

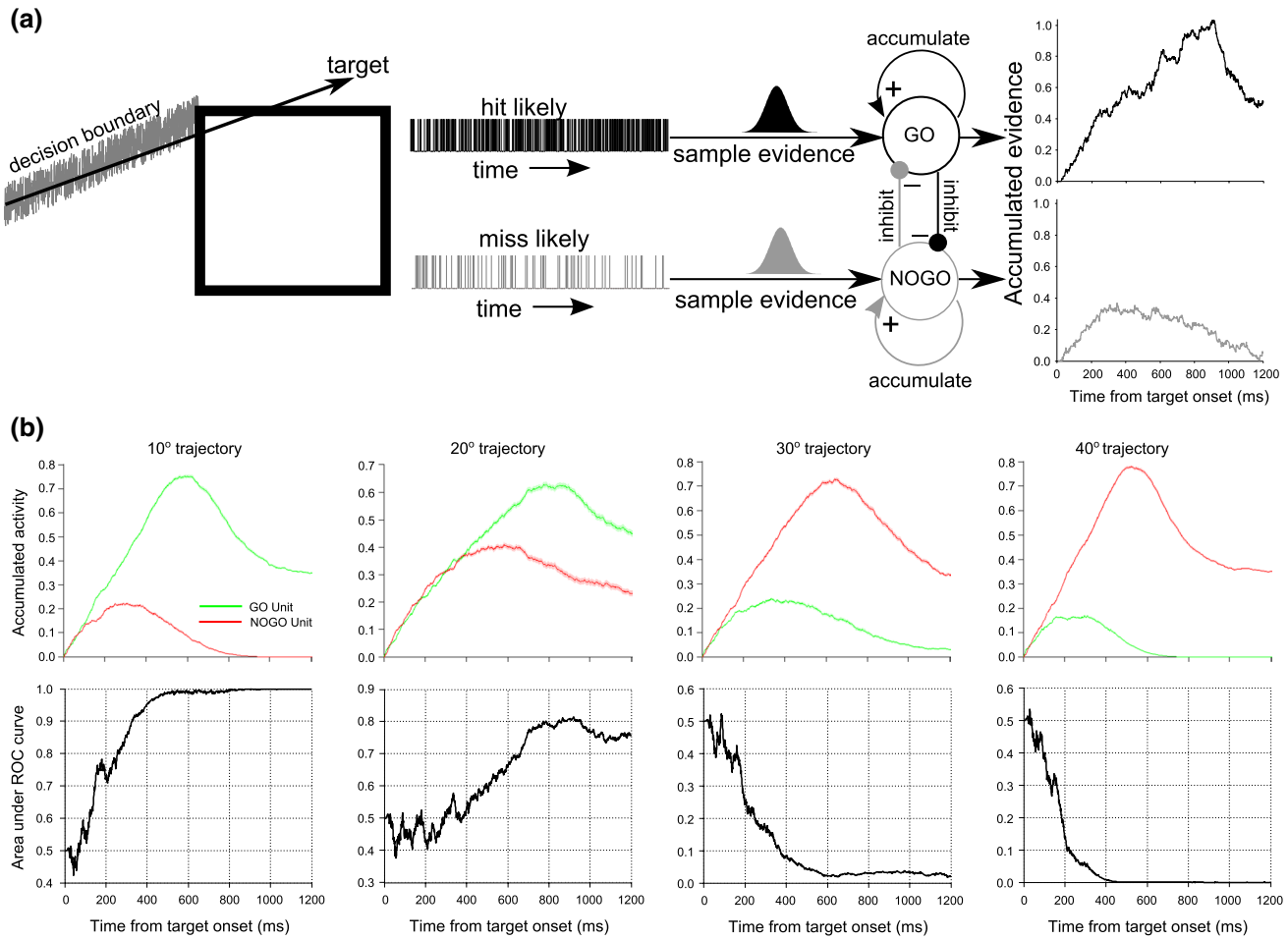

Fig. 5 **a** Simulation of the SEF activity during the oculomotor baseball task. The model compares the target trajectory with a noisy representation of the decision boundary conceptualized by an invisible line connecting the target origin with the nearest corner of the plate. At each time point, if the comparator determines that the target is likely to intersect the plate, it triggers the GO integrator to sample evidence from a Gaussian distribution, which is then accumulated in favor of a pursuit eye movement. If the comparator determines that the target is likely to bypass the plate, it triggers the NOGO integrator to sample evidence from the same distribution, which is then accumulated in favor of fixation. Triggering signals are shown as *arrays* of *small vertical lines* for GO (*black*) and NOGO (*gray*) integrators. At an instant of time, the integrators dissipate (or leak) information and inhibit each other with strength proportional to the evidence gathered up to that point of time. After reaching a fixed threshold, accumulated evidence dissipates rapidly. Time-varying accumulated evidence in the GO (*black*) and NOGO (*gray*) units during an example strike trial is shown at right. **b** *Black* and *gray lines* show average GO and NOGO activity, respectively, for 500 simulated trials (*top panel*). *Thin shaded regions* show the standard error of the mean activity. Areas under the ROC curves (*bottom panel*) were generated by comparing simulated GO and NOGO activity individually for four cardinal directions

increased activity for the agonist rule-state as did the neurons; however, unlike the neurons, activity of the model units rose at different rates for different trajectories invoking the same rule-state. Activity in the GO and NOGO units increased in the first epoch and decreased in the last epoch for both agonist and antagonist rule-states. However, in these epochs, the rate of change in activity in both model units statistically differed from the trend observed in neurons' activity.

Finally, we tested whether the model could account for deselection of the antagonist rule-state prior to selection of the agonist one. To this end, we randomly sampled a pair of trials, one difficult and one easy, which invoked the same rule-state. Then, separately for each integrator, we compared the accumulated activity between the two trials over time in a 100-ms-wide window sliding at 10-ms interval using a one-tailed Wilcoxon rank sum test. When the activity became significantly different ($P < 0.05$), and remained significantly different for at least 100 consecutive ms, we considered that time to be the deselection time for the antagonist rule-state and the selection time for the agonist rule-state. We repeated the test across 200 pairs of trials in each rule-state for both the GO and NOGO units. Figure 6c shows the cumulative distributions of deselection and

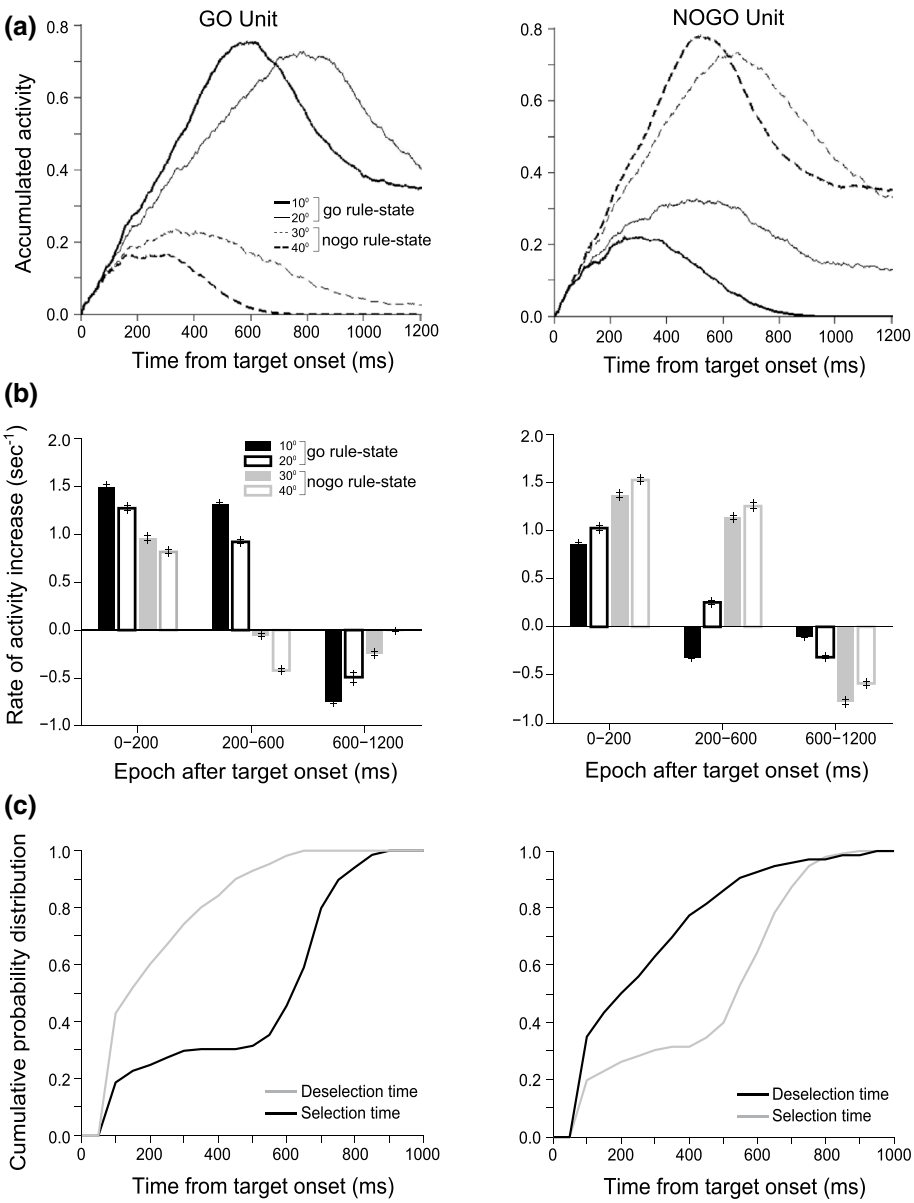

Fig. 6 **a** Average (±s.e.m) GO (*left*) and NOGO (*right*) activity during 500 simulated trials for each of the four target motion angles. **b** Average (±s.e.m) rate of change in GO (*left*) and NOGO (*right*) activity across all simulated trials is compared in three consecutive epochs (compare with Fig. 2g, h). **c** Cumulative distributions of time when GO (*left*) and NOGO (*right*) accumulators discriminated between motion directions specifying the agonist rule-state (selection time) and the antagonist rule-state (deselection time) (compare with Fig. 3e, f). The GO unit deselected the nogo rule-state (*gray*) before selecting the go rule-state (*black*), and the NOGO unit deselected the go rule-state (*black*) before selecting the nogo rule-state (*gray*)

selection times for the antagonist and agonist rule-states, respectively, for each unit. The average (±s.e.m) time to deselect the nogo rule-state by GO unit (224 ± 13 ms) was significantly earlier than that required to select the go rule-state (523 ± 20 ms) ($P < 0.001$), and the time to deselect the go rule-state by NOGO unit (281 ± 16 ms) was significantly earlier than that required to select the nogo rule-state (477 ± 18 ms) ($P < 0.001$).

Discussion

In this study, we present evidence that two complementary populations of neurons in the SEF discriminate between go and nogo rule-states in our ocular baseball task according to how certainly the trajectory of a moving target invokes a rule-state. One population of neurons increases activity to select the rule-state, while the other decreases activity to deselect the rule-state, possibly to increase the difference in overall activity between the go and nogo neurons allowing quicker discrimination between rule-states. This rapid decrease in activity might also serve to eliminate from further processing trajectories that would not be candidates for the behavior corresponding to the preferred rule-state. The main findings of this study are (1) SEF neurons deselect the non-preferred/antagonist rule-state before they select the preferred/agonist one, (2) the activity within the antagonist rule-state drops more rapidly for the trajectory that invokes the rule-state with more certainty. A computational model using a pair of integrators—one that accumulates evidence

in favor of pursuit and another that accumulates evidence in favor of fixation—accounts for the physiological phenomena observed in the SEF.

There is physiological evidence that SEF neurons contribute to smooth pursuit eye movement generation (Heinen 1995; Tian and Lynch 1995; Missal and Heinen 2001; Fukushima et al. 2004, 2011) and decision making (Coe et al. 2002; So and Stuphorn 2010). Neurons here not only signal an upcoming pursuit eye movement in a predictive fashion (Heinen and Liu 1997; de Hemptinne et al. 2008) but also contribute to the animal's choice—either to pursue or to maintain fixation (Kim et al. 2005; Shichinohe et al. 2009). However, SEF activity reflects the decision rule, and not the final decision, as SEF neurons continue to discriminate rule-states correctly even when the animal's behavioral choice does not comply with the rule-state (Yang et al. 2010; Heinen et al. 2011). The results from the present study complement these previous findings by suggesting a plausible neural mechanism for discriminating decision rule-states in the SEF and provide a computational framework supporting this mechanism.

Results from previous studies provide hints that rejecting irrelevant or non-rewarded stimuli or behaviors might be important for choosing between alternative actions. Concurrent activation of neural populations that encode multiple motor plans (Cisek and Kalaska 2010; Klaes et al. 2011) requires an 'inhibition-for-deselection' mechanism to resolve the competition (Cisek 2006, 2007, but also see Duque and Ivry 2009). Moreover, in many regions of the brain, activity is attenuated to signal anti-preferences in tasks that require selection of an action from alternatives (Motter 1994; Recanzone et al. 1997; Roitman and Shadlen 2002; Sato and Schall 2003; Hasegawa et al. 2004; Cisek and Kalaska 2005; Khayat et al. 2006; McPeek 2006; Bodis-Wollner 2008; Ding and Gold 2010; Hanks et al. 2011). For example, visually responsive neurons in the frontal eye field (FEF) decrease activity to deselect a target when it leaves their receptive fields in order to facilitate redirection of the end point of a saccade to the final location of the target (Murthy et al. 2009). Deselection also seems to be critical in ensuring that the effector of a movement is unambiguous, specifying between hands (Koch et al. 2006), or between eye and hand (Cui and Andersen 2007).

In the ocular baseball task, a decision criterion separates different motion directions into two groups, which results in the activation of two corresponding populations of neurons. Complementary populations of neurons have also been observed in other regions of the brain that are involved in categorical decision making. In a paradigm where alternative actions are chosen based on tactile information, two sets of neurons have been identified in both the medial premotor cortex (MPC) and primary motor cortex (M1) that segregate stimuli into 'faster' and 'slower' speed categories by either increasing or decreasing their activity between two levels (Romo et al. 1997; Salinas and Romo 1998). Additionally, two populations of neurons in the prefrontal and parietal cortices reflect feature-based categorization of visual stimuli (Freedman et al. 2001; Cromer et al. 2010; Roy et al. 2010; Freedman and Assad 2006). Recently, complementary populations of neurons in the FEF have been identified that exhibit a preference for 'higher' or 'lower' speeds of visual motion (Ferrera et al. 2009). Neurons in the superior colliculus (SC) have also been shown to categorize the direction of coherent moving dots to plan a forthcoming saccade (Horwitz et al. 2004).

We think that the SEF lies beyond regions that merely categorize sensory stimuli in the neural cascade. Rather, this area appears to interpret the rule of our task and serves as a link between areas that categorize sensory motion and those that execute the behavioral choice. Anatomically, the SEF is situated well for this as it receives input from the medial superior temporal (MST) area (Huerta and Kaas 1990), which has neurons that are tuned to the speed and direction of visual motion (Tanaka and Saito 1989; Orban et al. 1995; Duffy and Wurtz 1997a, b), and projects to brain areas that contribute more directly to the execution of pursuit eye movements, like the FEF (Keating 1991; Gottlieb et al. 1994; Tanaka and Fukushima 1998; Tanaka and Lisberger 2002), the SC (Krauzlis et al. 2000; Krauzlis 2001), and pontine nuclei in the brainstem (Shook et al. 1990; Suzuki et al. 2003; Dicke et al. 2004; Leichnetz et al. 1984). The presence of a relatively large number of 'go' neurons in the SEF may be intended to drive a variety of motor neurons in downstream areas, and plan pursuit eye movements with numerous kinematic attributes, while the fewer 'nogo' neurons may be adequate to suppress activity of those neurons and hold the gaze at the fixation point. We did not find a systematic pattern of spatial distribution of the two types of neurons. However, multiple neurons of one type often appeared along a track of penetration. Previous studies have also reported small samples of neurons in the SEF that had higher activity during fixation compared to neurons that had higher activity during smooth pursuit (Kim et al. 2005; Fukushima et al. 2004; Shichinohe et al. 2009). In fact, a recent study has shown a biased proportion of pursuit and fixation-related neurons in both the SEF and FEF (Fukushima et al. 2011).

Sequential sampling models account for neural activity and behavior in perceptual decision-making tasks (Smith and Ratcliff 2004; Ditterich 2010). These models employ separate integrators that accumulate evidence in favor of each alternative. When the evidence in an integrator reaches a threshold, the appropriate movement is triggered (reviewed in Gold and Shadlen 2007; Deco et al. 2012; Zhang 2012). A buildup of neuronal activity in the lateral

intra-parietal area (LIP), FEF, and SC is thought to underlie the evolving perceptual decision and saccade preparation that occurs during the task (Horwitz and Newsome 1999; Kim and Shadlen 1999; Shadlen and Newsome 2001; Bennur and Gold 2011; Ding and Gold 2011; Ratcliff et al. 2003, 2007; Gold and Shadlen 2003). Sequential sampling models have largely been applied to the results obtained in two-alternative forced-choice tasks. In these tasks, the animals must discriminate the net direction of moving dots, and signal their perceptual decision, for example, by making a saccade to one of two targets (e.g., Newsome and Paré 1988; Salzman et al. 1990; Feng et al. 2009). In sequential sampling models applied to these tasks, different directionally tuned neurons in the medial temporal (MT) area are represented by separate distributions of neural activity that is integrated over time. A saccade is generated in the corresponding direction when one of the competing integrators (hypothesized to exist in the LIP) gathers enough sensory evidence from MT neurons to rise above a pre-assigned threshold (Mazurek et al. 2003). A variant of the sequential sampling model, the leaky competitive accumulator (LCA) model, incorporates mutual inhibition between a pair of leaky integrators to simulate the performance and neural activity in decision-making tasks (Usher and McClelland 2001; Mcmillen and Holmes 2006; Bogacz et al. 2007).

In order to model our SEF data, we considered that unlike in the LIP (Roitman and Shadlen 2002), the FEF (Hanes and Schall 1996), or the SC (Munoz and Wurtz 1995; Jantz et al. 2013), neurons in the SEF do not increase activity to a threshold at the time when an eye movement is generated. Additionally, directional tuning of neurons neither in the SEF (Yang et al. 2010) nor in the areas that are richly connected to the SEF in relation to ocular pursuit, for example, the FEF (Huerta and Kaas 1990; Ono and Mustari 2009), the parietal area 7a (Bremmer et al. 1997; Sakata et al. 1983), and the dorsal part of the middle superior temporal area (Ono and Mustari 2006), is as prominent as in MT (Maunsell and Van Essen 1983a, b; Orban 2008). Our model was inspired by the LCA model, but is different from that model in several important ways such as: (1) it does not assume a ceiling value of activity (i.e., threshold) in order to make a decision, (2) the GO and NOGO integrators in our model sample sensory evidence from the same distribution, and (3) either the GO or NOGO integrators accumulate evidence at a given instant of time in anticipation of whether the motion direction will signal the rule-state for ocular pursuit or fixation, respectively.

Biophysically, realistic models that describe how decisions are made between two alternative actions also incorporate WTA circuitry (Wang 2002; Lo and Wang 2006; Albantakis and Deco 2011). For example, models consisting of interactive populations of integrate-and-fire neurons have been proposed to categorize tactile stimuli (Machens et al. 2005) and to make flexible visuomotor associations (Loh and Deco 2005). Mutual inhibition between a pair of integrators has been shown to be critical for preserving the order of saccade execution in a sequence (Ray et al. 2012) and for optimizing visual search performance (Purcell et al. 2012). More relevant to our study, a model with two mutually inhibited accumulators has been introduced as a 'linking proposition' (Teller 1984; Schall 2004), which describes the activity of movement neurons in the FEF during countermanding (Boucher et al. 2007). In this interactive race model, two stochastic processes (GO and STOP) compete to rise to a threshold to signal that a saccade should be either generated or withheld, respectively. Because of the sequential nature of GO and STOP signal initiation in this model, to withhold a saccade, the inhibition exerted on the GO signal by the STOP signal must be strong enough to cease the growth of the GO signal shortly after the STOP signal begins to rise.

Similar to the race model of saccade generation, our model incorporates a pair of GO and NOGO integrators, which for our model represent populations of strike and ball neurons in the SEF. Each integrator differentially accumulates evidence by recurrent self-excitation, and the integrators are coupled by mutual inhibition. The inhibitory coupling of the integrators was motivated by the observation that when the activity of strike neurons rises to specify a rule-state, the activity of ball neurons falls, and vice versa. A rule-state is discriminated when the differential activity between the two integrators reaches a predetermined value. Although the model does not embody a specific anatomical architecture, or account for the disparity in the numbers of strike and ball neurons, the simulations we conducted with it captured two essential elements of SEF activity during discrimination of the go/nogo rule-states: (1) the antagonist rule-state is deselected before the agonist rule-state is selected, and (2) deselection occurs more rapidly when motion direction invokes the antagonist rule-state more certainly. Since we did not record activity from strike and ball neurons simultaneously, we had no means to directly set the ratio of strengths with which an integrator representing one population of neurons inhibited another in the model. Therefore, we preferred to set the strength of mutual inhibition, along with other constant parameters of the model including leakage and supra-threshold dissipation, identical for both integrators. However, we cannot rule out the possibility of different weights for inhibition for go and nogo integrators, given the disparity in the number of neurons mentioned above. Mutual inhibition, which suggests that higher activity in one population results in greater suppression of activity in the other, and vice versa, might seem improbable at first glance, since the neural activity in difficult trials (20° and 30° trajectories) is higher than that in easy trials (10° and 40° trajectories) in both populations

of neurons. But a close inspection of the model dynamics shows that the net accumulated evidence by one integrator depends not only on inhibition by the other, but also on how long the integrator continues to accumulate evidence in favor of its preferred rule-state. For example, the NOGO integrator accumulates evidence for the nogo rule-state, and the GO integrator accumulates evidence for go rule-state longer for 20° trajectories than 10° trajectories because 20° trajectories pass through the noisy decision boundary longer than 10° trajectories. The same argument holds true for 30° and 40° trajectories.

Because the decision boundary that divides motion directions into the two categories that specify pursuit and fixation does not physically exist in the stimulus display, it must be constructed mentally. Therefore, we assumed a noisy representation of the boundary for the model. Although, to the best of our knowledge, there is no reported evidence of neurons encoding the relative distance of a moving object, recent studies show that prefrontal (BA 46 and 8) neurons compare and discriminate relative distances of static objects (Genovesio et al. 2011). This finding to some extent lends support to our assumption that either the GO or NOGO integrator can be enabled at a given instant during simulation based on the distance of the target from the decision boundary. Thus, our model describes a plausible mechanism that can discriminate motion directions following a criterion in order to decide between ocular pursuit and fixation.

Acknowledgments This study was supported by grants from National Eye Institute (EY-117720) and The Smith-Kettlewell Eye Research Institute.

References

Albantakis L, Deco G (2011) Changes of mind in an attractor network of decision-making. PLoS Comput Biol 7:e1002086

Asaad WF, Rainer G, Miller EK (1998) Neural activity in the primate prefrontal cortex during associative learning. Neuron 21:1399–1407

Asaad WF, Rainer G, Miller EK (2000) Task-specific neural activity in the primate prefrontal cortex. J Neurophysiol 84:451–459

Badre D, Kayser AS, D'Esposito M (2010) Frontal cortex and the discovery of abstract action rules. Neuron 66:315–326

Bengtsson SL, Haynes J-D, Sakai K, Buckley MJ, Passingham RE (2009) The representation of abstract task rules in the human prefrontal cortex. Cereb Cortex 19:1929–1936

Bennur S, Gold JI (2011) Distinct representations of a perceptual decision and the associated oculomotor plan in the monkey lateral intraparietal area. J Neurosci 31:913–921

Bodis-Wollner I (2008) Pre-emptive perception. Perception 37:462–478

Bogacz R, Usher M, Zhang J, McClelland JL (2007) Extending a biologically inspired model of choice: multi-alternatives, nonlinearity and value-based multidimensional choice. Philos Trans R Soc Lond B Biol Sci 362:1655–1670

Boucher L, Palmeri TJ, Logan GD, Schall JD (2007) Inhibitory control in mind and brain: an interactive race model of countermanding saccades. Psychol Rev 114:376–397

Brainard DH (1997) The psychophysics toolbox. Spat Vis 10:433–436

Bremmer F, Distler C, Hoffmann KP (1997) Eye position effects in monkey cortex. II. Pursuit- and fixation-related activity in posterior parietal areas LIP and 7A. J Neurophysiol 77:962–977

Britten KH, Shadlen MN, Newsome WT, Movshon JA (1992) The analysis of visual motion: a comparison of neuronal and psychophysical performance. J Neurosci 12:4745–4765

Bunge SA (2004) How we use rules to select actions: a review of evidence from cognitive neuroscience. Cogn Affect Behav Neurosci 4:564–579

Bunge SA, Kahn I, Wallis JD, Miller EK, Wagner AD (2003) Neural circuits subserving the retrieval and maintenance of abstract rules. J Neurophysiol 90:3419–3428

Chen LL, Wise SP (1995) Neuronal activity in the supplementary eye field during acquisition of conditional oculomotor associations. J Neurophysiol 73:1101–1121

Chen LL, Wise SP (1996) Evolution of directional preferences in the supplementary eye field during acquisition of conditional oculomotor associations. J Neurosci 16:3067–3081

Cisek P (2006) Integrated neural processes for defining potential actions and deciding between them: a computational model. J Neurosci 26:9761–9770

Cisek P (2007) Cortical mechanisms of action selection: the affordance competition hypothesis. Philos Trans R Soc Lond B Biol Sci 362:1585–1599

Cisek P, Kalaska JF (2005) Neural correlates of reaching decisions in dorsal premotor cortex: specification of multiple direction choices and final selection of action. Neuron 45:801–814

Cisek P, Kalaska JF (2010) Neural mechanisms for interacting with a world full of action choices. Annu Rev Neurosci 33:269–298

Coe B, Tomihara K, Matsuzawa M, Hikosaka O (2002) Visual and anticipatory bias in three cortical eye fields of the monkey during an adaptive decision-making task. J Neurosci 22:5081–5090

Cromer JA, Roy JE, Miller EK (2010) Representation of multiple, independent categories in the primate prefrontal cortex. Neuron 66:796–807

Cui H, Andersen RA (2007) Posterior parietal cortex encodes autonomously selected motor plans. Neuron 56:552–559

de Hemptinne C, Lefèvre P, Missal M (2008) Neuronal bases of directional expectation and anticipatory pursuit. J Neurosci 28:4298–4310

Deco G, Rolls ET, Albantakis L, Romo R (2012). Brain mechanisms for perceptual and reward-related decision-making. Progr Neurobiol. doi:10.1016/j.pneurobio.2012.01.010

Dicke PW, Barash S, Ilg UJ, Thier P (2004) Single-neuron evidence for a contribution of the dorsal pontine nuclei to both types of target-directed eye movements, saccades and smooth-pursuit. Eur J Neurosci 19:609–624

Ding L, Gold JI (2010) Caudate encodes multiple computations for perceptual decisions. J Neurosci 30:15747–15759

Ding L, Gold JI (2011) Neural correlates of perceptual decision making before, during, and after decision commitment in monkey frontal eye field. Cereb Cortex 22:1052–1067

Ditterich J (2010) A comparison between mechanisms of multi-alternative perceptual decision making: ability to explain human behavior, predictions for neurophysiology, and relationship with decision theory. Front Neurosci 4(184):1–24

Duffy CJ, Wurtz RH (1997a) Medial superior temporal area neurons respond to speed patterns in optic flow. J Neurosci 17:2839–2851

Duffy CJ, Wurtz RH (1997b) Planar directional contributions to optic flow responses in MST neurons. J Neurophysiol 77:782–796

Duque J, Ivry RB (2009) Role of corticospinal suppression during motor preparation. Cereb Cortex 19:2013–2024

Feng S, Holmes P, Rorie A, Newsome WT (2009) Can monkeys choose optimally when faced with noisy stimuli and unequal rewards? PLoS Comput Biol 5:e1000284

Ferrera VP, Yanike M, Cassanello C (2009) Frontal eye field neurons signal changes in decision criteria. Nat Neurosci 12:1458–1462

Freedman DJ, Assad JA (2006) Experience-dependent representation of visual categories in parietal cortex. Nature 443:85–88

Freedman DJ, Riesenhuber M, Poggio T, Miller EK (2001) Categorical representation of visual stimuli in the primate prefrontal cortex. Science 312:291–316

Fukushima J, Akao T, Takeichi N, Kurkin S, Kaneko CRS, Fukushima K (2004) Pursuit-related neurons in the supplementary eye fields: discharge during pursuit and passive whole body rotation. J Neurophysiol 91:2809–2825

Fukushima J, Akao T, Shichinohe N, Kurkin S, Kaneko CRS, Fukushima K (2011) Neuronal activity in the caudal frontal eye fields of monkeys during memory-based smooth pursuit eye movements: comparison with the supplementary eye fields. Cereb Cortex 21:1910–1924

Genovesio A, Tsujimoto S, Wise SP (2011) Prefrontal cortex activity during the discrimination of relative distance. J Neurosci 31:3968–3980

Gold JI, Shadlen MN (2003) The influence of behavioral context on the representation of a perceptual decision in developing oculomotor commands. J Neurosci 23:632–651

Gold JI, Shadlen MN (2007) The neural basis of decision making. Annu Rev Neurosci 30:535–574

Gottlieb JP, MacAvoy MG, Bruce CJ (1994) Neural responses related to smooth-pursuit eye movements and their correspondence with electrically elicited smooth eye movements in the primate frontal eye field. J Neurophysiol 72:1634–1653

Green DM, Swets JA (1966) Signal detectability and psychophysics. Wiley, New York

Hanes DP, Schall JD (1996) Neural control of voluntary movement initiation. Science 274:427–430

Hanks TD, Mazurek ME, Kiani R, Hopp E, Shadlen MN (2011) Elapsed decision time affects the weighting of prior probability in a perceptual decision task. J Neurosci 31:6339–6352

Hasegawa RP, Peterson BW, Goldberg ME (2004) Prefrontal neurons coding suppression of specific saccades. Neuron 43:415–425

Heinen SJ (1995) Single neuron activity in the dorsomedial frontal cortex during smooth pursuit eye movements. Exp Brain Res 104:357–361

Heinen SJ, Liu M (1997) Single-neuron activity in the dorsomedial frontal cortex during smooth-pursuit eye movements to predictable target motion. Vis Neurosci 14:853–866

Heinen SJ, Hwang H, Yang S (2011) Flexible interpretation of a decision rule by supplementary eye field neurons. J Neurophysiol 106:2992–3000

Horwitz GD, Newsome WT (1999) Separate signals for target selection and movement specification in the superior colliculus. Science 284:1158–1161

Horwitz GD, Batista AP, Newsome WT (2004) Representation of an abstract perceptual decision in macaque superior colliculus. J Neurophysiol 91:2281–2296

Huerta MF, Kaas JH (1990) Supplementary eye field as defined by intracortical microstimulation: connections in macaques. J Comp Neurol 293:299–330

Jantz JJ, Watanabe M, Everling S, Munoz DP (2013) Threshold mechanism for saccade initiation in the frontal eye field and superior colliculus. J Neurophysiol

Keating EG (1991) Frontal eye field lesions impair predictive and visually-guided pursuit eye movements. Exp Brain Res 86:311–323

Khayat PS, Spekreijse H, Roelfsema PR (2006) Attention lights up new object representations before the old ones fade away. J Neurosci 26:138–142

Kim JN, Shadlen MN (1999) Neural correlates of a decision in the dorsolateral prefrontal cortex of the macaque. Nat Neurosci 2:176–185

Kim YG, Badler JB, Heinen SJ (2005) Trajectory interpretation by supplementary eye field neurons during ocular baseball. J Neurophysiol 94:1385–1391

Klaes C, Westendorff S, Chakrabarti S, Gail A (2011) Choosing goals, not rules: deciding among rule-based action plans. Neuron 70:536–548

Koch G, Franca M, Del Olmo MF, Cheeran B, Milton R, Sauco MA, Rothwell JC (2006) Time course of functional connectivity between dorsal premotor and contralateral motor cortex during movement selection. J Neurosci 26:7452–7459

Krauzlis RJ (2001) Extraretinal inputs to neurons in the rostral superior colliculus of the monkey during smooth-pursuit eye movements. J Neurophysiol 86:2629–2633

Krauzlis RJ, Dill N (2002) Neural correlates of target choice for pursuit and saccades in the primate superior colliculus. Neuron 35:355–363

Krauzlis RJ, Basso MA, Wurtz RH (2000) Discharge properties of neurons in the rostral superior colliculus of the monkey during smooth-pursuit eye movements. J Neurophysiol 84: 876–891

Leichnetz GR, Smith DJ, Spencer RF (1984) Cortical projections to the paramedian tegmental and basilar pons in the monkey. J Comp Neurol 228:388–408

Lo CC, Wang XJ (2006) Cortico-basal ganglia circuit mechanism for a decision threshold in reaction time tasks. Nat Neurosci 9:956–963

Loh M, Deco G (2005) Cognitive flexibility and decision-making in a model of conditional visuomotor associations. Eur J Neurosci 22:2927–2936

Machens CK, Romo R, Brody CD (2005) Flexible control of mutual inhibition: a neural model of two-interval discrimination. Science 307:1121–1124

MacMillan NA, Creelman CD (1991) Detection theory: a user's guide. Cambridge University Press, Cambridge

Maunsell JH, Van Essen DC (1983a) Functional properties of neurons in middle temporal visual area of the macaque monkey. I. Selectivity for stimulus direction, speed, and orientation. J Neurophysiol 49:1127–1147

Maunsell JH, Van Essen DC (1983b) The connections of the middle temporal visual area (MT) and their relationship to a cortical hierarchy in the macaque monkey. J Neurosci 3:2563–2586

Mazurek ME, Roitman JD, Ditterich J, Shadlen MN (2003) A role for neural integrators in perceptual decision making. Cereb Cortex 13:1257–1269

Mcmillen T, Holmes P (2006) The dynamics of choice among multiple alternatives. J Math Psychol 50:30–57

McPeek RM (2006) Incomplete suppression of distractor-related activity in the frontal eye field results in curved saccades. J Neurophysiol 96:2699–2711

Missal M, Heinen SJ (2001) Facilitation of smooth pursuit initiation by electrical stimulation in the supplementary eye fields. J Neurophysiol 86:2413–2425

Mitz AR, Godschalk M, Wise SP (1991) Learning-dependent neuronal activity in the premotor cortex: activity during the acquisition of conditional motor associations. J Neurosci 11:1855–1872

Motter BC (1994) Neural correlates of attentive selection for color or luminance in extrastriate area V4. J Neurosci 14:2178–2189

Muhammad R, Wallis JD, Miller EK (2006) A comparison of abstract rules in the prefrontal cortex, premotor cortex, inferior temporal cortex, and striatum. J Cogn Neurosci 18:974–989

Munoz DP, Wurtz RH (1995) Saccade-related activity in monkey superior colliculus. I. Characteristics of burst and buildup cells. J Neurophysiol 73:2313–2333

Murthy A, Ray S, Shorter SM, Schall JD, Thompson KG (2009) Neural control of visual search by frontal eye field: effects of unexpected target displacement on visual selection and saccade preparation. J Neurophysiol 101:2485–2506

Newsome WT, Paré EB (1988) A selective impairment of motion perception following lesions of the middle temporal visual area (MT). J Neurosci 8:2201–2211

Ono S, Mustari MJ (2006) Extraretinal signals in MSTd neurons related to volitional smooth pursuit. J Neurophysiol 96:2819–2825

Ono S, Mustari MJ (2009) Smooth pursuit-related information processing in frontal eye field neurons that project to the NRTP. Cereb Cortex 19:1186–1197

Orban GA (2008) Higher order visual processing in macaque extrastriate cortex. Physiol Rev 88:59–89

Orban GA, Lagae L, Raiguel S, Xiao D, Maes H (1995) The speed tuning of medial superior temporal (MST) cell responses to optic-flow components. Perception 24:269–286

Oster M, Douglas R, Liu SC (2009) Computation with spikes in a winner-take-all network. Neural Comput 21:2437–2465

Pouget P, Emeric EE, Stuphorn V, Reis K, Schall JD (2005) Chronometry of visual responses in frontal eye field, supplementary eye field, and anterior cingulate cortex. J Neurophysiol 94:2086–2092

Purcell BA, Schall JD, Logan GD, Palmeri TJ (2012) From salience to saccades: multiple-alternative gated stochastic accumulator model of visual search. J Neurosci 32:3433–3446

Ratcliff R, Cherian A, Segraves MA (2003) A comparison of macaque behavior and superior colliculusneuronal activity to predictions from models of two-choice decisions. J neurophysiol 90(3):1392–1407

Ratcliff R, Hasegawa YT, Hasegawa RP, Smith PL, Segraves MA (2007) Dual diffusionmodel for single-cell recording data from the superior colliculus in a brightness-discrimination task. J neurophysiol 97(2):1756–1774

Ray S, Pouget P, Schall JD (2009) Functional distinction between visuomovement and movement neurons in macaque frontal eye field during saccade countermanding. J Neurophysiol 102:3091–3100

Ray S, Bhutani N, Murthy A (2012) Mutual inhibition and capacity sharing during parallel preparation of serial eye movements. J Vis 12(3):17

Recanzone GH, Wurtz RH, Schwarz U (1997) Responses of MT and MST neurons to one and two moving objects in the receptive field. J Neurophysiol 78:2904–2915

Roitman JD, Shadlen MN (2002) Response of neurons in the lateral intraparietal area during a combined visual discrimination reaction time task. J Neurosci 22:9475–9489

Romo R, Merchant H, Zainos A, Hernández A (1997) Categorical perception of somesthetic stimuli: psychophysical measurements correlated with neuronal events in primate medial premotor cortex. Cereb Cortex 7:317–326

Roxin A, Ledberg A (2008) Neurobiological models of two-choice decision making can be reduced to a one-dimensional nonlinear diffusion equation. PLoS Comput Biol 4(3):e1000046

Roy JE, Riesenhuber M, Poggio T, Miller EK (2010) Prefrontal cortex activity during flexible categorization. J Neurosci 30:8519–8528

Sakata H, Shibutani H, Kawano K (1983) Functional properties of visual tracking neurons in posterior parietal association cortex of the monkey. J Neurophysiol 49:1364–1380

Salinas E, Romo R (1998) Conversion of sensory signals into motor commands in primary motor cortex. J Neurosci 18:499–511

Salzman CD, Britten KH, Newsome WT (1990) Cortical microstimulation influences perceptual judgements of motion direction. Nature 346:174–177

Sato TR, Schall JD (2003) Effects of stimulus-response compatibility on neural selection in frontal eye field. Neuron 38:637–648

Schall JD (2004) On building a bridge between brain and behavior. Annu Rev Psychol 55:23–50

Schlag J, Schlag-Rey M (1987) Evidence for a supplementary eye field. J Neurophysiol 57:179–200

Shadlen MN, Newsome WT (2001) Neural basis of a perceptual decision in the parietal cortex (Area LIP) of the rhesus monkey. J Neurophysiol 86:1916–1936

Shichinohe N, Akao T, Kurkin S, Fukushima J, Kaneko CRS, Fukushima K (2009) Memory and decision making in the frontal cortex during visual motion processing for smooth pursuit eye movements. Neuron 62:717–732

Shook BL, Schlag-Rey M, Schlag J (1990) Primate supplementary eye field: I. Comparative aspects of mesencephalic and pontine connections. J Comp Neurol 301:618–642

Smith PL, Ratcliff R (2004) Psychology and neurobiology of simple decisions. Trends Neurosci 27:161–168

So N-Y, Stuphorn V (2010) Supplementary eye field encodes option and action value for saccades with variable reward. J Neurophysiol 104:2634–2653

Song JH, McPeek RM (2010) Roles of narrow- and broad-spiking dorsal premotor area neurons in reach target selection and movement production. J Neurophysiol 103:2124–2138

Suzuki DA, Yamada T, Yee RD (2003) Smooth-pursuit eye-movement-related neuronal activity in macaque nucleus reticularis tegmenti pontis. J Neurophysiol 89:2146–2158

Tanaka M, Fukushima K (1998) Neuronal responses related to smooth pursuit eye movements in the periarcuate cortical area of monkeys. J Neurophysiol 80:28–47

Tanaka M, Lisberger SG (2002) Role of arcuate frontal cortex of monkeys in smooth pursuit eye movements. I. Basic response properties to retinal image motion and position. J Neurophysiol 87:2684–2699

Tanaka K, Saito HA (1989) Analysis of motion of the visual field by direction, expansion/contraction, and rotation cells clustered in the dorsal part of the medial superior temporal area of the macaque monkey. J Neurophysiol 62:626–641

Teller DY (1984) Linking propositions. Vision Res 24:1233–1246

Tian JR, Lynch JC (1995) Slow and saccadic eye movements evoked by microstimulation in the supplementary eye field of the cebus monkey. J Neurophysiol 74:2204–2210

Usher M, McClelland JL (2001) The time course of perceptual choice: the leaky, competing accumulator model. Psychol Rev 108:550–592

Wallis JD, Miller EK (2003) From rule to response: neuronal processes in the premotor and prefrontal cortex. J Neurophysiol 90:1790–1806

Wallis JD, Anderson KC, Miller EK (2001) Single neurons in prefrontal cortex encode abstract rules. Nature 411:953–956

Wang XJ (2002) Probabilistic decision making by slow reverberation in cortical circuits. Neuron 36:955–968

White IM, Wise SP (1999) Rule-dependent neuronal activity in the prefrontal cortex. Exp Brain Res 126:315–335

Yang S-n, Hwang H, Ford J, Heinen S (2010) Supplementary eye field activity reflects a decision rule governing smooth pursuit but not the decision. J Neurophysiol 103:2458–2469

Zhang J (2012) The effects of evidence bounds on decision-making: theoretical and empirical developments. Front Psychol 3